

**Tracing High-Redshift Black Holes with
ALMA in Atomic Cooling Lines**
Bachelor Thesis Astronomy

Margriet van der Laan - University of Groningen
Supervisor: Prof. Dr. Marco Spaans - Kapteyn Astronomical Institute

May 8, 2009

Abstract

Nowadays it is known that galaxies with Super Massive Black Holes (SMBH), $\geq 10^8 M_{\odot}$, do exist [Häring & Rix (2004)]. However, the process behind the formation of these SMBH is not quite well understood. A SMBH must be formed through accretion from (less) massive seed black holes in the early universe, to become like the present-day SMBHs which are at this moment in the nuclei of a lot of galaxies [Bromm & Loeb (2003)]. If we are able to detect these young high-redshift black holes we make a huge step forward in the understanding of this process. X-rays are produced by the accretion of mass onto the black holes. Spaans & Meijerink (2008) already showed that the molecules CO and H₂ can be used to trace this young population of accreting massive black holes through the X-ray irradiation of ambient gas. In this small research a mini-quasar is considered at high-redshift, which for simplicity contains a black hole that radiates at the Eddington luminosity. NGC 1068 is taken as a reference system and is hypothetically put at high-redshift, e.g. $z = 10$. In this work it is investigated how one can observe accreting black holes at redshifts $5 \leq z \leq 10$ through the atomic cooling lines [CII]158 and [OI]63 μm . The atomic cooling lines are driven by the X-rays and are accessible to ALMA, the Atacama Large Millimeter/submillimeter Array. ALMA is now being built and will be fully operational in 2013. Moreover, using the Press & Schechter formalism the number of expected halos which one can detect with ALMA is given for completeness [Schleicher et al. (2008)].

Contents

1	Introduction	2
1.1	Supermassive high-redshift black holes	2
1.2	Magorrian relation	5
1.3	Cooling and Heating	7
1.4	Far-UV and X-ray dominated regions	11
2	ALMA	13
3	Press & Schechter formalism	17
3.1	Seed black holes	17
3.2	Press & Schechter formalism	18
4	Discussion and Conclusion	21

Chapter 1

Introduction

This small research is about the possibility of “Tracing High-Redshift Black Holes with ALMA in the Atomic Cooling Lines [CII]158 and [OI]63?”. This introduction chapter gives the necessary background information about high-redshift black holes and atomic cooling lines. Chapter 2 explains more about observing with ALMA, the Atacama Large Millimeter/submillimeter Array. ALMA is an astronomical instrument composed of 66 antennas of 12 meters each, located on the Chajnantor plain at 5000 meter altitude. ALMA will operate at millimeter wavelengths, where the Earth’s atmosphere above a high, dry site is largely transparent, and will provide astronomers a high sensitivity and resolution. This chapter also gives a prediction, taking NGC 1068 as a reference galaxy, about observing a high-redshift black hole with the atomic cooling lines [CII]158 and [OI]63 μm using ALMA. Chapter 3 introduces the Press & Schechter formalism and predicts how many quasars one expects to find with ALMA. Finally, chapter 4 covers the discussion and the conclusion. Here the possibilities of the telescope APEX, the Atacama Pathfinder Experiment, related to this research are discussed. APEX is a modified ALMA prototype antenna as a single dish on the high altitude site of Llano de Chajnantor.

1.1 Supermassive high-redshift black holes

That the galaxies are seen at high-redshift ($z > 2$) means they are very distant and we see them as they existed in the early universe. In order to see galaxies at high-redshift they have to be very bright and therefore be Active Galactic Nuclei (AGN). In this small research the focus is on galaxies with a super massive black hole (SMBH) at high-redshift. A SMBH is a black hole with a mass of the order of $\geq 10^8 M_{\odot}$.

Quasars (quasi-stellar radio sources or QSOs) are a type of AGN, which are powered by a super massive black hole. A SMBH is normally surrounded by an accretion disk and two jets (see figure 1). Quasars thus produce a very large amount of (radiative and mechanical) energy due to accretion and are the most luminous objects known in the universe. The high-accretion is possible, because at high-redshift there is a lot of matter to accrete due to the built-up and mergers of galaxies in the early universe. Seen from a different point of view, a SMBH whenever fuelled at a sufficient rate, displays quasar-like activity. If

one looks from above on a quasar, then one sees only the clear accretion disk. Looking from the side through the big accretion disk gives a view with a lot of dust, which obscures the sight. One should keep this in mind when a quasar is observed. Quasars can be detected over the entire observable electromagnetic spectrum including radio, infrared, optical, ultraviolet, X-ray and even gamma rays. The features of quasars at high-redshift give us a better understanding of how galaxies form, grow and how black holes play a role in their development. In particular the accretion signatures of the young black holes, so-called mini-quasars, would contribute to the understanding of the early universe. Quasar redshifts are measured from the strong spectral lines that dominate their spectra. These lines are brighter than the continuous spectrum, so they are called ‘emission’ lines. Emission lines of hydrogen (mainly of the Lyman series and Balmer series), Helium, Carbon, Magnesium, Iron and Oxygen are the brightest lines. The atoms emitting these lines range from neutral to highly ionized (i.e. many of the electrons are stripped off the ion, leaving it highly charged). This wide range of ionization shows that the gas is highly irradiated by the quasar. The quasar distribution tells us that at least some massive black holes formed early. Quasars with black hole masses of the order of $10^9 M_{\odot}$ and with supersolar metallicities are even observed at redshift 6 [Fan et al., 2001, Schleicher et al. 2008].

Seyfert galaxies are another type of AGN, which have extremely bright nuclei and their spectrum shows broad and narrow emission lines. The black hole has an accretion disk around it where the particle velocities are very high (500 - 4000 km/s), these particles show mostly Keplerian motions and a large turbulent dispersion. The broad emission lines in its spectrum come from the accretion disk and thus from very close to the black hole. The narrow emission lines come from the outer part of the AGN where the particle velocities are lower (see figure 1). We distinguish two types of Seyfert galaxies; the first type is a Seyfert 1 galaxy, these galaxies show spectra with broad and narrow emission lines. The second type is a Seyfert 2 galaxy, these galaxies show in their spectra only narrow emission lines. The broad component in the spectra of a Seyfert 2 galaxy is obscured by dust and/or by our viewing angle on the galaxy. NGC 1068 is an example of a Seyfert 2 galaxy and will act as a reference galaxy in this work.

Accretion disk The accretion disks and gas jets of black holes behave in the same way as those of ultra-dense objects such as neutron stars and white dwarfs. One thus needs to make a distinction in some way between these two different kind of objects when one observes an accretion disk. The easiest way is to identify a star through a hot spot where the accretion flow hits the surface of the star. A black hole does not have a solid surface and thus does not show a hot spot. A black hole, and therefore its accretion disk, can be identified because of the large stellar motions around the accretion disk (see also section 1.2). The existing black hole in our own Milky Way is for example determined like this.

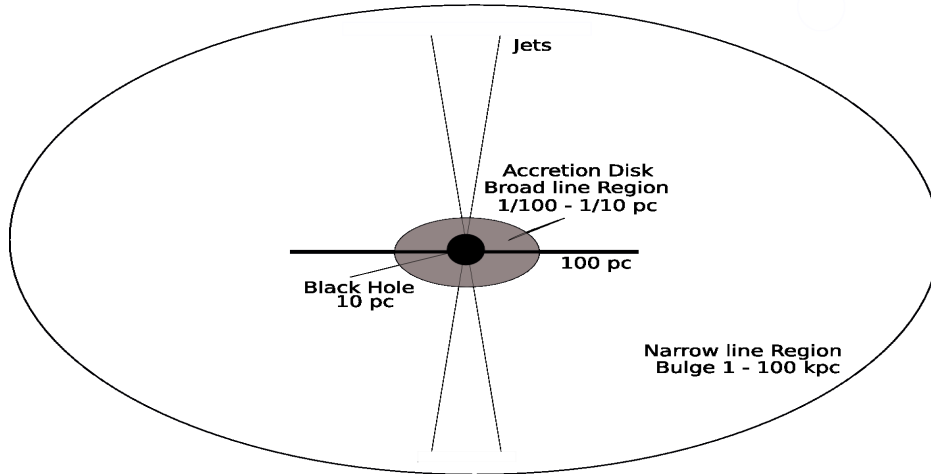


Figure 1: A schematic picture of a quasar with its scales.

Eddington luminosity In this small research we are assuming a black hole is accreting at the Eddington rate. The Eddington luminosity, L_{Edd} , is the maximum surface luminosity of a star where the gravitational force inwards equals the radiation pressure outwards, assuming hydrostatic equilibrium and spherical symmetry. The Eddington luminosity is thus a kind of maximum luminosity and therefore often called the Eddington-limit (which holds for high mass stars, $M \geq 50 M_{\odot}$). To get a formula for the Eddington luminosity, start with the formula for the radiation pressure:

$$P_{rad} = \frac{aT^4}{3} \quad (1.1)$$

Also, use the equation for radiative transport:

$$\frac{dT}{dr} = -\frac{3\kappa_r\rho}{4acT^3}F_r. \quad (1.2)$$

Now, knowing that the flux $F_r = L_r / 4\pi r^2$ and κ is the mean radiative opacity, one finds that

$$\frac{dP}{dr} = -\frac{k\rho L_r}{4\pi cr^2}. \quad (1.3)$$

Next, use $dP = -g\rho dr$, where $g = GM / R^2$, and $\rho = MR^{-3}$ (approximately). We are allowed to make these assumptions, because we are looking at the surface of the total accretion disk of a black hole. Now, one can find the following equation:

$$L = \frac{4\pi cG}{\kappa}M. \quad (1.4)$$

In the Eddington-limit, the mass-luminosity relation is thus: $L \propto M$. The exact value of the Eddington luminosity depends on the chemical composition of the gas layer and the spectral energy distribution of the emission. Larger luminosities imply a radiative pressure too strong to be balanced by the gravitational

force. The black hole will therefore radiate at the maximum luminosity L_{Edd} , which becomes bigger if M grows. Whenever black holes accrete efficiently and release the gravitational energy as radiation, the luminosity can be estimated with the Eddington luminosity as [Schleicher et al. , 2008]:

$$L_{Edd} = 3.3 \times 10^4 \left(\frac{M_{BH}}{M_{\odot}} \right) L_{\odot} \quad (1.5)$$

Also sub-Eddington and super-Eddington luminosities may occur. Clumpiness (a lot of matter under a small surface) and over-pressure can cause a super-Eddington luminosity and therefore high accretion is possible. However in theory the Eddington luminosity is a *maximum* luminosity, therefore typical luminosities are in fact sub-Eddington. A sub-Eddington luminosity can occur when there are a lot of particles like protons, they can absorb energy in stead of giving the energy to electrons which radiate more easily. Another condition which can cause a sub-Eddington is when some energy goes into mechanical feedback like jets and outflows rather than radiation. The luminosity of NGC 1068 is for example 50% of the Eddington-limit [Schleicher et al. (2008)].

1.2 Magorrian relation

Magorrian et al. (1998) show evidence that Massive Dark Objects (MDOs) are present in the centres of nearby galaxies. The MDOs are probably black holes, since star clusters of the required mass and size are otherwise difficult to construct and maintain, on top of this such a massive system would be very unstable. Additionally inactive quasar remnants which are now black holes are expected to be common in galaxy centres. A correlation between the black hole mass and the hot stellar component of the galaxy is the very tight relation between M_{bh} and the stellar velocity dispersion σ of the bulge stars [N. Häring & H. Rix (2004)]. The velocity dispersion is the spread of velocities of stars in the galaxy, which can be estimated by measuring the radial velocities of selected stars. Once the velocity distribution is known, the cluster’s mass can be calculated using the virial theorem. The *virial theorem* states that for gravitationally bound systems in equilibrium, the total energy is equal to one half the time-averaged potential energy:

$$2E_i = -\Omega. \quad (1.6)$$

Here E_i is the internal energy and Ω is the total potential energy. The virial theorem thus provides a way of estimating the mass of star clusters, galaxies, or clusters of galaxies from observations of the movement of individual members. See the paragraph below for the virial temperature. Moreover a relation is found between the mass of the central black hole, M_{bh} , and the stellar mass of the surrounding spheroid/bulge of the galaxy, M_{bulge} . This is the so-called Magorrian relation. One can see this relation as the growing galaxy in some way “knows about” or “feels” the central black hole, or vice versa the black hole “feels” the stellar mass of the galaxy. Direct M_{bh} estimates and M_{bulge} determinations [N. Häring & H. Rix (2004)] give an implied median black hole mass fraction (at bulge masses of $\sim 5 \times 10^{10} M_{\odot}$) of :

$$M_{bh} : M_{bulge} = (1.4 \pm 0.4) * 10^{-3} \quad (1.7)$$

The *Magorrian relation* connects the velocity dispersion and therefore the mass of the galactic bulge with M_{bh} [Schleicher et al. (2008)]. On the other hand if one knows the M_{bulge} , it can be used to determine velocities inside the galaxy, using the fact that GM/R is proportional to v^2 . Considering this relationship the presence of the central black hole may thus play a key role in the formation and evolution of a galaxy.

Virial Temperature We define a cloud's virial temperature T_{vir} to be the mean temperature at which the cloud would satisfy the virial theorem. Recall that in an ideal gas the mean-square velocity is

$$\langle v^2 \rangle = \frac{3k_B T}{\mu m_p} \quad (1.8)$$

k_B is the Boltzmann constant, μ is the mass per particle in the cloud, T is the temperature and m_p is the mass of a proton. An equation for T_{vir} will follow using the virial theorem, the kinetic energy $K = (1/2)M\langle v^2 \rangle$ (here also the internal energy) and $r_h = 0.4r_g$. Here r_h is the median radius, defined as the radius within which lies half the system's mass, and r_g is the gravitational radius.

$$\langle v^2 \rangle = \frac{-\Omega}{M} \cong 0.4 \frac{GM}{r_h} \quad (1.9)$$

Use equation (1.10) for getting an equation for the temperature T :

$$T = 0.40 \frac{GM}{r_h} \frac{\mu m_p}{3k_B}. \quad (1.10)$$

Rewriting this gives:

$$T_{vir} \approx 0.13 \frac{GM\mu m_p}{k_B r_h} \approx 6.8 \times 10^5 \mu \left(\frac{M}{10^{11} M_\odot} \right) \left(\frac{10 \text{ kpc}}{r_h} \right) K. \quad (1.11)$$

One can deduce that the condition for gas in a cloud to become gravitational unstable is $T_0 \ll T_{vir}$, where T_0 is the temperature of the cloud. From the virial temperature of the gas around a black hole, one can calculate how fast the BH is accreting (through rewriting the observable flux and calculating the real luminosity). For cooling processes below temperatures $T \approx 10^4$ K, where the processes are dominated by molecular hydrogen H_2 and hydrogen deuteride HD , one can calculate T_{vir} as follows:

$$T_{vir} = 1.98 \times 10^4 \left(\frac{\mu}{0.6} \right) \left(\frac{M}{10^8 h^{-1} M_\odot} \right)^{2/3} \left(\frac{\Omega}{\Omega_z} \frac{\Delta}{18\pi^2} \right)^{1/3} \left(\frac{1+z}{10} \right) K \quad (1.12)$$

Here μ is the mean molecular weight and Δ is the collapse overdensity. In this equation the overdensity and redshift are included, in contrast with equation (1.13), which is a more simple version. Equation (1.14) holds thus for small virial temperatures around 10^4 K.

Jeans length and mass Thermal energy loss allows a cloud to contract. At the critical length, the *Jeans length* λ_J , the cloud neither expands nor contracts.

At this length the thermal energy per particle is in equilibrium with the gravitational work per particle. The Jeans length is thus the critical size at which a molecular cloud becomes gravitationally unstable and begins to collapse.

$$\lambda_J = \sqrt{\frac{15k_B T}{4\pi G \mu \rho}} \approx 0.062 \text{ kpc} \left(\frac{T}{200 \text{ K}}\right)^{1/2} \left(\frac{n}{10^4 \text{ cm}^{-3}}\right)^{-1/2}. \quad (1.13)$$

The *Jeans mass* is the minimum mass of a molecular cloud for collapsing under its own gravity and the maximum mass value for a cloud that can be in equilibrium. In other words the maximum mass of a cloud that is stable under the influence of gravity. The virial theorem tells us that when the internal energy is smaller than the gravitational energy of a molecular cloud it will collapse under its own gravity:

$$M_J = \left(\frac{5k_B T}{G \mu m_p}\right)^{3/2} \left(\frac{3}{4\pi \rho}\right)^{1/2} \approx 45 M_\odot T^{3/2} n^{-1/2}. \quad (1.14)$$

M_J is thus proportional to $T^{3/2}$ and $\rho^{-1/2}$.

1.3 Cooling and Heating

One can only detect an isolated black hole by its interactions with other material. ALMA can detect emissions from atoms and molecules that are excited in interstellar gas close to the accreting black hole. An accreting black hole which grows in mass is actually a big potential well, attracting mass in its surroundings. Before matter falls into an accreting black hole it will send off radiation and release its gained energy by means of cooling. The atomic cooling lines that are driven by the X-rays due to the accretion are accessible to ALMA. The accretion onto a black hole provides in this way the energy source for an AGN. In this way fast accretion means thus high and efficient cooling. In this section the cooling and heating processes are described. Also the free fall time and the cooling time are treated.

The cooling and heating processes In the case of an accreting black hole the radiation emitted is röntgenradiation (X-rays). The accretion disk of the quasar is thus the source of X-rays. The thermal balance of the accretion disk consists roughly of two steps; first, due to X-rays, ionization occurs which heats up the material and second the material cools, after collisional excitation, by means of atomic fine-structure lines.

X-rays An accretion disc is normally thin and stable. However turbulent viscosity can occur in the accretion disc around a black hole, by example caused by magnetic rotation instabilities. This turbulent viscosity brings on a redistribution of the angular momentum in the disc. This happens by means of dissipation and this gives rise to thermalization and the production of X-rays. The accretion disc thus warms and radiates in X-rays indirect due to turbulent viscosity. Seen from another point of view: if matter falls inwards it must lose not only gravitational energy but also lose angular momentum. Since the total angular momentum of the disc is conserved, the angular momentum loss of the

mass falling into the center has to be compensated by an angular momentum gain of the mass far from the center. In other words, angular momentum should be transported outwards for matter to accrete. The X-rays cause heating processes and the composition of the gas cloud determines the cooling processes. The heating and cooling processes search an equilibrium at a specific temperature T_{gas} . One detects the cooling luminosity and therefore one can know the total X-ray luminosity:

$$L_{cooling} = L_{heating} = \epsilon \times L_{X-rays} \quad (1.15)$$

Here ϵ is the heating efficiency and lies between 0.1 and 0.3, for molecular cooling it is known that $\epsilon \approx 30\%$. Thus, if heating = cooling and one knows the cooling luminosity through observation one can calculate the total X-ray luminosity. The accretion process will lead to the emission of X-rays that impact thermal, ionization and chemical balance of the gas in the halo, leading to an X-ray dominated region (see section 1.4).

Heating process A neutral atom is ionized whenever an electron is liberated with sufficient energy, either through radiation or collisions. The high-energy photons ($\geq 1\text{keV}$), which are produced due to the accretion, collide with H , H_2 or/and He and ionize them. This process is the first ionization and produces high-energetic, very fast electrons:



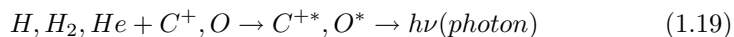
Part of the kinetic energy of these very fast (photo)electrons cause secondary ionizations. These secondary ionizations are far more important for H , H_2 or He than the direct or primary ionization: if the primary ionization happens once, the secondary ionization happens around 26 times. The secondary ionization:



The very fast electrons also transfer their energy to many other thermal electrons, i.e. Coulomb heating:



Cooling process After the ionizations and the Coulomb heating, which heat the gas, collisional excitation occurs and the gas cools. An atom may be excited to a higher level in two ways: radiation excitation or collisional excitation. When a photon is absorbed by an atom one calls it radiation excitation and this process produces absorption lines in the spectrum, but does not cool the gas. Collisional excitation can actually cool the gas. A free particle (electron or another atom) collides with an atom, giving part of its energy to the atom (no photons are involved). If the energy of the particle (electron or another atom) corresponds to the energy of a bound-bound transition, the atom is collisional excited to a higher state. Such an atom returns to its ground state by emitting photons, producing emission line spectra in the process and cooling the gas. The actually cooling mechanism for the atomic cooling lines of [OI]63 and [CII]158 μm is as follows:



The photon with energy $h\nu$ is, if it is redshifted to a longer wavelength, detectable with ALMA. At a metallicity of $\sim 10^{-2}$, cooling by means of atomic fine-structure lines contributes about half to the total cooling. At metallicities of $Z/Z_{\odot} < 10^{-3}$ the cooling consists of molecular cooling by H_2 and HD. However we see that quasars do have already solar metallicity at redshift $z = 6$ [Pentericci et al. (2002), Juarez et al. (2009)] and thereby are able to cool using metals. The metallicity Z/Z_{\odot} is important, because it determines the dominant coolants in a specific cloud. The cooling and heating processes in a specific cloud will reach a state of equilibrium and a equilibrium temperature T_{gas} which is dependent of the composition of the gas.

There are a lot of different cooling mechanisms and the mechanism described above, which uses the fine-structure lines [CII]158 and [OI]63 μm , is one of many. The best known cooling process is through the emission line Lyman α of HI. Cooling is also possible through H_2 , HD and molecules (e.g. CO, H_2 , OH and H_2O). If the metallicity is zero the dominant coolants are HI, HD and H_2 . Lyman α cools optimally at a temperature of 10^4 K. H_2 cools at a much lower temperature, because of this lack in temperature Lyman α is dominant for a lot of HI gas clouds and these gas clouds have therefore typically temperatures of 10^4 K. By looking at different and more cooling lines of one particular cloud the physical characterization of the cloud is better. [OI]63 and [CII]158 μm are two important cooling lines and contribute for a better and total understanding of the cooling processes near super massive black holes.

Through detecting the photons send out by cooling, one can know the kinetic temperature T_{kin} of the cloud. To determine T_{kin} one has to do excitation analysis of multiple lines. As mentioned above, one looks at different cooling lines and therefore one knows restricted temperatures of the cloud. This is because coolants always have a maximum and a minimum temperature at which they can cool. One combines the restricted temperatures, the number density n and the column density N and looks at the proportions between these observables. For example, if the temperature is higher, the cloud would send off more photons. But if you observe a bigger column of the cloud, the number of photons send off is also higher. In the same way, if the particle number density is higher (and not the temperature or a bigger column), more photons are generated. The cooling process follows a Boltzmann distribution and is thus proportional to $\exp[h\nu/kT]$.

Free fall time One can determine a *Cooling time* and a *Free fall time*. If the cooling time $\tau_{cooling} < \tau_{ff}$ then the cloud collapses under its own gravitation and stars can be formed. On the other hand if the $\tau_{cooling} > \tau_{ff}$ then the cloud does *not* collapse. Below the cooling and free fall time are defined, these are important to understand the circumstances under which the BHs were formed. The free fall time τ_{ff} (sometimes called the dynamical time) is the time that a body or cloud takes to collapse under its own gravity if there are no other forces present, i.e. if no other forces exist to oppose the collapse. The free fall time τ_{ff} can be calculated using Kepler's third law. Kepler's third law depends only on the semi-major axis (take $R/2$) and not on the eccentricity (take $\epsilon = 1$) of the cloud. For a pure radial motion the time for a body to fall inward to the central mass, turn around and come back at its original position is the same

as the period of a circular orbit of radius $R/2$:

$$t_{orbit} = \frac{2\pi}{\sqrt{GM}} \left(\frac{R}{2}\right)^{3/2} = \frac{\pi R^{3/2}}{\sqrt{2GM}} \quad (1.20)$$

To obtain the free fall time one can just divide t_{orbit} by two, because τ_{ff} is the time it takes for a body to fall inward. Remember:

$$\rho = \frac{M}{V} = \frac{3M}{4\pi R^3}. \quad (1.21)$$

Use $\rho = nm_H$, where n is the total number of free particles per cm^3 in the interstellar gas, to get:

$$\tau_{ff} = \frac{t_{orbit}}{2} = \frac{\pi R^{3/2}}{2\sqrt{2GM}} \quad (1.22)$$

$$\tau_{ff} = \sqrt{\frac{3\pi}{32Gnm_H}} \approx 0.347 \text{ Myr} \left(\frac{n}{10^4 \text{ cm}^{-3}}\right)^{-1/2}. \quad (1.23)$$

Cooling time and Coolants The cooling process stops when the gas has too low energy for collisional excitation. This means the formation of stars depends on the ability of interstellar gas to cool and form dense molecular clouds. The cooler the gas is, the better the conditions for starformation are. Quantum mechanically is defined that metals can cool better than molecular hydrogen, mainly because metals have a permanent dipole moment. The intensity of the coolingrate is proportional to the Einstein coefficient of the particle, A_{ij} . Subsequently, A_{ij} is proportional to the dipole moment. Whenever a gas cloud contains a lot of particles with an electric dipole moment, it will thus cool better and faster. This implies that metals stimulate the starformation. Furthermore it is generally recognized that the overall galaxy mass (and following the Magorrian relation also the black hole mass) is correlated with its metallicity [Schleicher et al. (2008)]. There are three different types of discrete energy levels for molecules: [1] electronic transitions (these are the most common, atoms have also electronic transitions), [2] vibrational energy states and [3] (pure) rotational energy states. J is the rotating quantum number and a transition $J = 16 \rightarrow J = 15$ means losing rotation energy. The cooling time $\tau_{cooling}$ is the time a cloud takes to radiate away the bulk of its internal energy. Below is an equation for $\tau_{cooling}$ which uses the internal energy ($3/2 k_B T$):

$$n \frac{d}{dt} \left(\frac{3}{2} k_B T\right) = -\frac{3k_B(T - T_E)}{2\tau_{cooling}}. \quad (1.24)$$

The earliest formed gas with temperatures $T \geq 10^4$ K are mostly cooled by Lyman α emission of neutral atomic hydrogen (HI 121.6 nm) and helium (He 30.4 nm). Below this temperature, which is the case in minihalos with virial temperatures $T_{vir} \lesssim 10^4$ K, the cooling process is dominated by molecular hydrogen (H_2) and hydrogen deuteride (HD). H_2 cooling is for this reason important in primordial gas. Molecular hydrogen does not have a permanent electric dipole moment while the HD molecule has and this makes HD a better coolant than H_2 : the first excited rotational state of H_2 lies at ~ 500 K and the first excited rotational state of HD lies at a temperature of ~ 150 K. However remember there is very little HD , because the relation deuterium/hydrogen is about 10^{-5} ,

and therefore HD is only important at very low temperatures. In the very first gaseous objects with masses of $\sim 10^5 M_\odot$, just above the cosmological Jeans mass, fragmentation into stars is possible because of their low virial temperature (hundreds of kelvins). Namely through the formation of molecular hydrogen, H_2 , which cools efficiently via rotational-vibrational transitions even at these low temperatures. H_2 is collisionally dissociated at $\gtrsim 2000$ K. However, there could be a destructive flux of UV photons [Bromm and Loeb (2003)]. See also the table below for details.

Coolant	Temperature (K)	Metallicity (Z)	Density (cm^{-3})
HI (and He)	$\geq 10^4$	$\ll 10^{-3} Z_\odot$	$\gtrsim 10^8$
H_2	500 ($\gtrsim 200$)	$\ll 10^{-3} Z_\odot$	$10^3 - 10^4$
HD	(\lesssim) 200	$\ll 10^{-3} Z_\odot$	$10^4 - 10^6$
Metals: CII, OI	92, 224	$\geq 10^{-3} Z_\odot$	$10^3, 10^5$

Table 1: Different coolants with their temperatures, metallicities and densities.

When the gas is enriched by metals one has to take into account the cooling from the fine-structure lines of metals. If this is the case, metallicities between 10^{-3} and 1.0 solarmetallicity Z_\odot are considered since $\ll 10^{-3} Z_\odot$ is quite like a zero-metallicity and supersolar values appear unlikely for the bulk of the very high-redshift gas. The energy difference between the 3P_1 and 3P_2 levels of [OI] 63 μm is 2×10^{-2} eV, corresponding to a temperature of ~ 224 K. For carbon, the energy difference between the $^3P_{3/2}$ and $^2P_{1/2}$ levels of [CII] 158 μm is 7.93×10^{-3} eV, corresponding to a temperature of ~ 92 K.

1.4 Far-UV and X-ray dominated regions

Gas clouds in the inner kpc of many galaxies are exposed to intense radiation, which can originate from an active galactic nucleus (AGN), a starburst region or both [Meijerink & Spaans (2005)]. We distinguish the Photon Dominated Region (PDR) and the X-ray Dominant Region (XDR). The PDR is a far-ultraviolet ($6.0 \lesssim E \lesssim 13.6$ eV) dominant region. Here O and B stars, thus starbursts, dominate the radiation and therefore turn cloud surfaces into PDRs. The XDR is created by hard X-rays ($10 \text{ keV} \lesssim E \lesssim 100 \text{ keV}$) from black hole environments (AGN), X-rays can penetrate much deeper into cloud volumes than far-ultraviolet (FUV) photons. Although one region can dominate energetically over the other, the very different physics (surface vs. volume, cooling and heating processes etc.) requires that both regions should be considered simultaneously in each galaxy. When one observes a galaxy with an accreting BH one observes an XDR dominating a PDR; just like the AGN is dominant in NGC 1068. For this work it is important to know the differences between a PDR and an XDR. The cooling, heating and chemical processes contain and show these differences.

PDRs and XDRs emit different kinds of lines in their *spectra*. From Meijerink & Spaans (2005): PDRs emit finestructure lines of [CII]158 and [OI]63 μm , rotational lines of CO, rotational-vibrational and pure rotational lines of H_2 (also many H_2O lines as well as many broad mid-IR features associated with PAHs (Polycyclic Aromatic Hydrocarbons)). In PDRs, the bulk of H_2 is converted into atomic hydrogen at the edge and CO to neutral carbon into ionized carbon. XDRs emit brightly in [OI]63, [CII]158, [SiII]35 and the [FeII]1.26, 1.64 μm

lines as well as the 2 μm rotational-vibrational H_2 transitions. The abundance of neutral carbon in XDRs is elevated compared to that in PDRs and the chemical transitions from H to H_2 and C^+ to C to CO are smoother.

The dominant *heating and cooling processes* are also different for PDRs and XDRs. In PDRs the dominant heating process, up to a column density of $N_H \approx 10^{22} \text{ cm}^{-2}$, is photo-electric emission from grains. At high column densities ($N_H > 10^{22.5} \text{ cm}^{-2}$), [OI]63 μm absorption and gas-grain heating are important. The dominant cooling processes in PDRs are [OI]63 and [CII]158 μm cooling lines and gas-grain cooling. Unlike PDRs, XDRs are mostly heated by direct photo-ionization, i.e. Coulomb heating with thermal electrons. When X-rays are absorbed, fast electrons are produced that lose energy through collisions with other electrons, as well as with H and H_2 . These fast electrons collisionally excite H and H_2 , which subsequently emit Lyman α and Lyman-Werner band photons, respectively. These photons in turn are capable of ionizing atoms such as C or ionize and dissociate molecules such as H_2 and CO. Coulomb heating is important at column densities of $N_H > 10^{23} \text{ cm}^{-2}$. For smaller ionization fractions, ionization heating is important. Because the heating in XDRs is mostly driven by photo-ionization, the heating efficiency is close to unity. This is opposed to that in PDRs, where the photo-electric heating efficiency is of the order of 0.3-1.0%. XDRs are exposed to X-rays as well as FUV photons, unlike PDRs. As mentioned above XDR photons penetrate much deeper into a cloud than FUV photons, therefore high temperatures are maintained ($10^2 - 10^3 \text{ K}$) to much greater depths into the clouds. For each X-ray energy there is a characteristic depth where photon absorption occurs. So, for different spectral shapes, one has different thermal and chemical structures through the cloud [Spaans & Meijerink 2005]. All these features are strongly dependent on the column densities of the regions. Because XDR photons have much more energy and penetrate much deeper into a cloud than PDR photons, PDRs show already around $N_H \approx 10^{22} \text{ cm}^{-2}$ a lot of variation in the abundances of atoms and molecules. XDRs show variation around $N_H \approx 10^{24} \text{ cm}^{-2}$.

Spaans & Meijerink 2005 compare CO lines for making a distinction between a PDR and a XDR. The X-rays drive a low-metallicity ion-molecule chemistry that leads to the formation and excitation of CO and H_2 in $100 \text{ K} < T \leq 1000 \text{ K}$ gas [Spaans & Meijerink (2008)]. The accretion process of a BH will lead to the emission of X-rays that impact the thermal, ionization, and chemical balance of the gas in the halo, leading to an XDR.

Chapter 2

ALMA

The Atacama Large Millimeter Array (ALMA) is a cooperation between Europe, east-Asia and North America and is situated in Chile. Absorption by atmospheric lines (mainly by water vapor) is the greatest problem facing sub-millimeter astronomy. At an altitude of 5100 meter, Cerro Chajnantor in the dry Chilean Atacama desert is one of the best places for submillimeter astronomy on earth. ALMA consists of a giant array of about 66 (sub)millimeter antennas with a diameter of ~ 12 meter. One observes in the (sub)millimeter for more understanding of the cold gas in galaxies that give rise to the formation of stars and planets. One of the ideas of this small research is that galaxies with a SMBH at high-redshift can be observed indirect by ALMA. ALMA can detect emissions from atoms and molecules that are excited in interstellar gas close to the accreting black hole. In this report NGC 1068 is used as a reference galaxy and its properties are used for the calculations and expectations as it is observed by ALMA at a redshift of $6 \leq z \leq 10$.

NGC 1068 NGC 1068 is a Seyfert 2 galaxy at a distance of about 14.4 Mpc. Seyfert galaxies are, as mentioned in section 1.1, a subclass of AGN with nuclei that produce spectral line emission from highly ionized gas and contain a black hole. The BH of NGC 1068 is $\sim 10^7 M_{\odot}$. AGN NGC 1068 is studied well in different wavelengths and with high resolution. For example X-ray photons are observed and its molecular disk has been studied through emission from different species (in particular molecular CO and fine structure lines). Further, the continuum emission and the distribution of dust has been measured in further studies, thus stellar and gaseous dynamics and the galactic gravitational potential are examined. The inner radio jet can also be detected. Given this amount of detail, NGC 1068 provides an excellent test case for the inner structure of active galaxies [Schleicher et al. (2008)]. One can look for other galaxies that perhaps can serve as a reference system, for example NGC 5044 (an elliptical galaxy) or NGC 4027 (a merger), but they do not have features better than NGC 1068 to represent an AGN at high-redshift. In strong contrast to the optical image, 80 percent of the ALMA detected galaxies will lie at high redshifts. Although high-redshift galaxies are more distant, much of the dominant emission from warm dust is redshifted into the ALMA frequency bands. On

the ALMA website¹ one finds the three science goals of ALMA. This research project is connected to science goal 1: “Detect spectral line emission from CO or CII in a normal galaxy like the Milky Way at a redshift of $z = 3$, in less than 24 hours of observation”.

Wavelength range The observing wavelength range of ALMA is $400 \mu\text{m} - 3 \text{ mm}$. Using the relation $\lambda = v/f$ and the speed of light ($3 \times 10^8 \text{ m/s}$) one can calculate that a wavelength of $\lambda = 10^{-3} \text{ meter}$ corresponds to $3.0 \times 10^{11} = 300 \text{ GHz}$. The observing frequency range is thus $84 - 720 \text{ GHz}$. ALMA has seven different receiver bands to observe, running from band 3 to band 9. Look for example at band 3; this band covers the frequencies $84 - 116 \text{ GHz}$ and this corresponds to $3.6 - 2.6 \text{ mm}$ in wavelength.

The [CII]158 and [OI]63 μm cooling lines are observable with ALMA if they are emitted by a galaxy at high-redshift. From Spinoglio et al. (2005) one knows the lines [OI]63.184 μm and [CII]157.741 μm are observed from NGC 1068. Use the following formula for calculating the observed wavelength λ_o , λ_e is the emitted wavelength:

$$z = \frac{\lambda_o}{\lambda_e} - 1. \quad (2.1)$$

Now put NGC 1068 hypothetical at redshift $z = 10$:

$$\lambda_o([\text{OI}]63) = (10 + 1) \times 0.063 \text{ mm} = 0.693 \text{ mm}.$$

$$\lambda_o([\text{CII}]158) = (10 + 1) \times 0.158 \text{ mm} = 1.738 \text{ mm}.$$

Both wavelengths (0.69 and 1.74 mm) fall in the wavelength range of ALMA. This means NGC 1068 will be observable by ALMA if the galaxy lies at redshift 10. If the galaxy lies at redshift 5 the observed wavelengths are 0.32 and 0.79 mm, for [OI]63 and [CII]158 μm respectively, and are thus detectable with ALMA.

Band (nr)	Wavelength range (mm)	Angular Resolution baseline = 18 km (max) (arc sec)	Line sensitivity (mJy)
3	2.6 - 3.6	0.034	8.9
4	1.8 - 2.4	0.023	9.1
5	1.4 - 1.8	0.018	150
6	1.1 - 1.4	0.014	13
7	0.8 - 1.1	0.011	21
8	0.6 - 0.8	0.008	63
9	0.4 - 0.5	0.005	80

Table 2: ALMA specifications

Observing flux The field of view is the angular area viewed by the telescope and is determined by the antenna size and the observing frequency. The baseline D is several kilometers ($\leq 18 \text{ km}$) and the position of the antennas is variable. ALMA has a field of view which is determined by the $\sim 12 \text{ meter}$ of the different telescopes and is $\sim (30'')^2$ at 1 mm. The field of view is independent of the array configuration.

¹The website of ALMA: www.eso.org/sci/facilities/alma

The *spectral resolution* of a frequency spectrum is a measure of its power to resolve features in the electromagnetic spectrum. The spectral resolution R can be expressed in terms of velocity resolution; it describes the difference between velocities Δv . The definition is $R = c / \Delta v$, where c is the speed of light. A velocity resolution of 0.01 km/s corresponds to a spectral resolution of $R = 3 \times 10^7$. The output will look like data cubes (versus the uv-plane). The velocity resolution depends on the width of the frequency channels, which are the spectral resolution elements. The spectral resolution of ALMA is thus very high and ALMA is able to measure very small velocity differences.

The *spatial resolution* is the ability to distinguish between two closely spaced objects in an image. The spatial resolution of ALMA depends on the observing frequency and the maximum baseline of the array, following the λ/D scaling. The spatial resolution is the restricting factor for accurate observations, and thus not the spectral resolution. The spatial resolution of ALMA is about $1/100''$ at $\lambda = \sim 1$ mm: $\lambda / D = 1.0 \times 10^{-3} / 18000 = 5.56 \times 10^{-8}$ radians, which is $0.01''$. In the most compact configurations ($D = 200$ meters), resolutions range from $0.4''$ at 675 GHz to $2.8''$ at 110 GHz (one can use the same calculation as before). Remember:

$$1 \text{ radian} = (180 / \pi)^\circ \text{ (degree)} \text{ and } 1^\circ \text{ (degree)} = 60' \text{ (arcmin)} = 3600'' \text{ (arcsec)}$$

With a spatial resolution of $1/100''$ ALMA is able to distinguish scales of ~ 40 pc (the scalesize) at redshift 10: First calculate that the co-moving radial distance for a galaxy at $z = 10$ is $r = 9145.2$ Mpc. Second remember the following formula to calculate the angular size distance D_A :

$$D_A = \frac{r}{1+z} \quad (2.2)$$

Thereafter calculate the angle on the sky using:

$$\theta = \frac{\text{scalesize}}{D_A} \quad (2.3)$$

$$\theta = \frac{\text{scalesize} \times (1+z)}{r} = \frac{40 \times 11}{9145.2 \times 10^6} = 4.81 \times 10^{-8} \text{ radians}$$

$$4.81 \times 10^{-8} \text{ radians} \approx 0.01''$$

These calculations imply that a scalesize of 40 pc at redshift $z = 10$ will cover $0.01''$ on the sky, which is thus observable with ALMA. Remember due to cosmology a scalesize of 40 pc putted at higher redshift first looks smaller and smaller on the sky, but after a certain redshift the scalesize begins to appear bigger (due to the angular size distance D_A wich has a peak at a certain redshift). If one takes this scale as the radius of a disk, the disk will cover:

$$\pi \times (4.56 \times 10^{-8} \text{ radians})^2 = 6.53 \times 10^{-15} \text{ steradians.}$$

The redshifted wavelength 0.693 mm of [OI]63 is observable in band 8 of ALMA. Band 8 has a line sensitivity of

$$63 \text{ mJy} = 63 \times 10^{-29} \text{ J s}^{-1} \text{ m}^{-2} \text{ Hz}^{-1} = 63 \times 10^{-26} \text{ erg s}^{-1} \text{ cm}^{-2} \text{ Hz}^{-1}$$

for 1 sigma in 1 minute integration time. Remember:

1 Jy (Jansky) = 10^{-26} watt m⁻² Hz⁻¹.

The flux (power per unit area) of [OI]63 of NGC 1068 at its real distance ~ 15.2 Mpc ($z \approx 0.0038$) is

$$156 \times 10^{-13} \text{ ergs s}^{-1} \text{ cm}^{-2} \text{ [Spinoglio et al. (2005)]}$$

Use the following equation to calculate the flux received from NGC 1068 at $z = 10$:

$$Flux = \frac{Luminosity}{4\pi D_L^2} \quad (2.4)$$

Here D_L is the luminosity distance and the flux decreases with D_L^2 . The luminosity distance at $z = 10$ is $D_L = 100590.6$ Mpc, which gives a flux of

$$3.56 \times 10^{-19} \text{ erg s}^{-1} \text{ cm}^{-2}.$$

The luminosity distance and the co-moving radial distance are calculated for a universe with $H_0 = 75$ and $\Omega_{vac} = 73$. Take $\Delta v = 3000$ m/s. $\lambda_o = 0.693$ mm gives a frequency f of 4.33×10^{11} Hz. Together this gives:

$$\Delta f = \frac{\Delta v}{c} \times f_0 = 10^{-5} \times 4.33 \times 10^{11} \text{ Hz} = 4.33 \times 10^6 \text{ Hz} \quad (2.5)$$

Divide the flux received from NGC 1068 at $z = 10$ by this Δf to get the same units as the sensitivity:

$$3.56 \times 10^{-19} \text{ erg s}^{-1} \text{ cm}^{-2} / 4.33 \times 10^6 \text{ Hz} = 82 \times 10^{-27} \text{ erg s}^{-1} \text{ cm}^{-2} \text{ Hz}^{-1}$$

$$82 \times 10^{-27} \text{ erg s}^{-1} \text{ cm}^{-2} \text{ Hz}^{-1} = 8.2 \text{ mJy}$$

A 3σ detection is wanted and since the signal-to-noise (S/N) ratio is proportional to $t^{1/2}$ one has to integrate for $10^2 \times 3^2 = 900$ minutes (15 hours). By integrating for 900 minutes S/N is $\sqrt{(900) \times (82 \times 10^{-27}) / (63 \times 10^{-26})} = 3.9$ is almost a 4σ detection.

In table 3 the fluxes (in mJy) from [OI]63 and [CII]158 μm are calculated for NGC 1068 at redshift 6, 8 and 10. In order to do the calculations for [CII]158 μm one needs to know the flux for [CII]158 μm from NGC 1068 at its real distance [Spinoglio et al. (2005)]:

$$216 \times 10^{-13} \text{ ergs s}^{-1} \text{ cm}^{-2}.$$

The table also shows in which band the different redshifted wavelengths are detectable with ALMA. This is important because the different bands have different line sensitivities, see table 2. For example band 5 has a very high line sensitivity of 150 mJy compared to band 6 which has a very low line sensitivity of 13 mJy. Obviously this is a direct consequence for the integration time that is needed for a 3σ detection.

Redshift z (Luminosity distance D_L in Mpc)	[OI]63			[CII]158		
	λ_o (mm)	Band (nr)	Flux (mJy)	λ_o (mm)	Band (nr)	Flux (mJy)
10 (100591 Mpc)	0.69	8	8.2	1.74	5	28
8 (77908 Mpc)	0.57	8/9	14	1.42	5	48
6 (55808 Mpc)	0.44	9	27	1.11	6	93

Table 3: Observed fluxes from [OI]63 and [CII]158 μm for NGC 1068 at different redshifts.

Chapter 3

Press & Schechter formalism

3.1 Seed black holes

The accretion onto the super massive black holes can provide the energy source for the active galactic nuclei, as is mentioned in section 1.1. The questions remain are: how are these SMBH formed, how did they evolve from their less massive seed black holes and in what kind of way do they impact the evolution of galaxies. Two processes [Spaans & Meijerink (2008)] which are believed to play a role in the formation of seed black holes, from which large black holes may form through accretion, are [1] seeds as the remnants of Population III stars [Abel et al. (2000)] and [2] the (singular) collapse of massive pre-galactic halos [Bromm & Loeb (2003) and Spaans & Silk (2006)]. As mentioned and treated in chapter 1 the growth of seed black holes to larger sizes involves accretion that roughly follows an Eddington rate and requires the incorporation of feedback effects [Silk & Rees (1998)].

Process [1] is the most simple scenario to form quasars with black holes; they have grown from the remnants of the first stars, which are believed to be very massive and whose black hole remnants could grow further by accretion. Population III stars are the very first stars, they are massive ($< 100 M_{\odot}$) and very hot stars. They are formed from the collapse of the primordial gas into dark matter minihalos. The formation for population III.1 stars is H_2 cooling, for population III.2 stars the formation is HD and H_2 cooling. There are no population III stars left and they are by definition metal free. Population II stars are the second generation stars. They are effected by the radiation of previously formed stars. Population II.2 stars are less massive than population II.1 stars. Unless population III stars are very massive, they hardly can end up in the observed supermassive black holes at $z \sim 6$. Radiative feedback from the stellar progenitor can delay accretion and a super-Eddington accretion is needed to grow to a SMBH.

Super massive black holes are actually too massive to be formed by hierarchical structure. Moreover at redshift $z = 6$ for example the Hubble time is $T_H \lesssim 10^9$ year, which is a very short time to construct a SMBH by accretion (unless a mega-super-Eddington accretion is possible). Process [2] is therefore an al-

ternative scenario and tries to give a solution to this problem: SMBHs are not formed from population III stars but were formed at once: **singular collapse**. Once singular collapse black holes are formed, the final black hole mass is increased during hierarchical merging processes and SMBH are formed. Mergers of galaxies and black holes provide a continuing supply of gas. Gas dissipation and accretion feed the central black hole. However this scenario can also give some problems, for instance one can think of the cloud fragmenting due to H_2 cooling or non-zero metallicity [Schleicher et al. (2008)].

Feedback We distinguish positive and negative feedback. In response to a perturbation, a negative feedback system will limit the output of the system to re-establish equilibrium. Positive feedback is, in contrast, a feedback in which the system responds in the same direction of the perturbation, resulting in amplification of the original signal instead of stabilizing the signal. The SMBH formed by singular collapse can have positive or negative feedback on starformation. One can think of several reasons why the first baryonic clouds (masses in the range of 10^5 to $10^6 M_\odot$) did not undergo fragmentation into stars. Silk & Rees (1997) argued the hypothesis that black hole formation and growth, rather than starformation, characterizes the earliest stages of formation. For example, in the absence of magnetic flux, cloud collapse may have been far more catastrophic than it is the case at the present epoch (positive feedback). The most important reasons for the first objects to form in the universe are SMBH and not stars, is that during subsequent mergers the holes could grow and exert a negative feedback on starformation. A high massive black hole inhibits star formation in its host halo by blowing gas out, but on the other hand the ejected gas may eventually pile up in a cool shell that fragments.

3.2 Press & Schechter formalism

The *gravitational instability theory* explains how stars, galaxies and clusters (i.e. the structure of the universe) are formed from a homogeneous and isotropic universe. This theory tells that the early universe had small fluctuations and that these fluctuations suffered under gravitational forces. The cosmological model nowadays used is the Cold Dark Matter model. Primordial density perturbations on a small scale appear to have a much higher amplitude than those on large scales. This leads to the conclusion that small clumps are the first to collapse and form structures and they then build up to larger structures by mergers and the accretion of matter. This process is called *hierarchical structure formation*. The Press & Schechter (PS) formalism is a powerful model of hierarchical structure formation. The PS formalism is used to estimate the number of collapsed objects as a function of mass at any given time (redshift z), due to gravity only. In other words the PS formalism describes the formation of galaxies and clusters of galaxies, by self-similar gravitational condensation. Self-similar means that the functional form of the mass distribution is maintained even as the characteristic scale of condensations gets larger and larger. Norman & Spaans (1996) give an equation for the abundance of halos $n(M, z)$ with mass between M and $M + dM$. To get an idea how the number of halos

is calculated, this is equation is as follows:

$$n(M, z) = \left(\frac{2}{\pi}\right)^{1/2} \left(\frac{\rho_0}{M^2}\right) y \frac{d \log y}{d \log M} \exp\left(\frac{-y}{2}\right) \quad (3.1)$$

Where $y = \delta_c(1+z)/\sigma(M)$, take $\delta_c = 1.68$ (the critical density) and for $\sigma(M)$ an expression for a standard CDM cosmology. The Sheth-Tormen formalism [Sheth et al. (2001)] is a modified version of the Press & Schechter formalism and predicts the co-moving number density of halos with different masses, $dn/d \log(M_h)$, where M_h is the halo mass. Schleicher et al. (2008) used the correlation between the black hole mass M_{bh} and the velocity dispersion σ given by Tremaine et al. (2002):

Redshift	$M_{bh} = 10^6 M_\odot$	$M_{bh} = 10^7 M_\odot$
20	0.0003	0
15	0.005	0.0001
12	0.02	0.001
10	0.03	0.002
8	0.06	0.005
6	0.08	0.01

Table 4: The co-moving number density of halos [Mpc^{-3}] that contain black holes of $10^6 M_\odot$ and $10^7 M_\odot$ for different redshifts. Adopted from figure 1 from Schleicher et al. (2008).

Schleicher et al. (2008) suggest an observational strategy to find potential AGN at high-redshift with line emission using ALMA. The black hole mass is a good indicator for the evolutionary stage of the quasar host galaxy, in particular with respect to the Magorrian relation and the expected metallicity. They estimate an expected number of 1 – 10 sources for ALMA with a field of view of $\sim (1')^2$, see for details table 5 and on the next page figure 2.

Redshift	Sources $M_{BH} \geq 10^6 M_\odot$	Sources $M_{BH} \geq 10^7 M_\odot$
10	3	0.2
9	5	0.3
8	7	0.5
7	9	0.8
6	10	1.0

Table 5: The number of expected sources for different black hole masses at redshifts 6 – 10. Here is a field of view adopted of $(1')^2$, an active quasar fraction of 20% and a redshift interval of $\Delta z = 0.5$. Used is figure 9 from Schleicher et al. (2008).

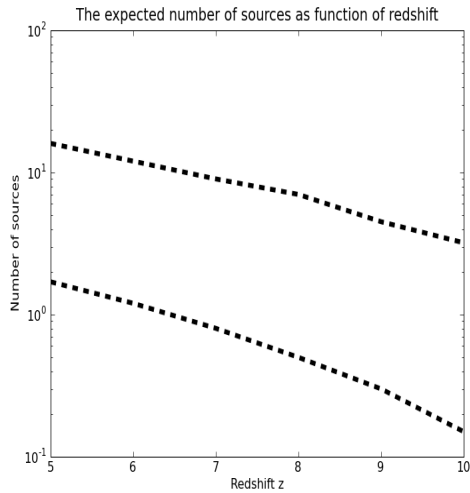


Figure 2: The upper and lower line represent the expected number of sources with a $M_{bh} \geq 10^6 M_\odot$ and with a $M_{bh} \geq 10^7 M_\odot$, respectively, as a function of redshift.

Cosmology Earlier times are more energetic times. The universe is homogeneous and isotropic on scales of 100 Mpc. The luminous portions of galaxies are typically much smaller than the dark halos in which they are embedded. In the usual scenario for galaxy formation, this is because the baryonic component of a galaxy radiates away energy, in the form of photons, and slides to the bottom of the potential well defined by the dark matter. The baryonic gas then fragments to form stars or SMBH are formed. After the Dark Ages, re-ionization begins (probably at $z \sim 15-20$) and galaxies/quasars start to form. It is completed at $z = \sim 6$ and during the re-ionization is the crucial time where the SMBH could have formed.

Chapter 4

Discussion and Conclusion

Discussion The telescope ALMA is good for a very accurate observation of an accreting black hole at high-redshift. However, this is true given that ALMA has to integrate for at least a few hours and therefore by forehand the position of the black hole on the sky has to know. For this reason ALMA is not perfect to search the sky for high-redshift super massive black holes; the telescope APEX¹ may be. The Atacama Pathfinder Experiment, APEX, is a modified ALMA prototype antenna as a single dish on the high altitude site of Llano de Chajnantor. APEX just consists of only one dish, therefore it will only be able to find black holes with masses $\geq 10^7 M_{\odot}$. However, because it has just a single dish it can investigate the sky and search for more high-redshift SMBH. APEX thus serves as a pathfinder for ALMA by performing wide-field observations. Later, ALMA will use these observations for followup studies in all of its wavelength ranges. Surveys with APEX will be an outstandingly efficient means of finding target sources for ALMA. The most interesting of the newly discovered objects (by APEX) will then be studied with greater spatial resolution and in their spectral line emission (by ALMA).

Much of the stellar light emerging from massive star formation regions is immediately absorbed by the surrounding dusty clouds. For this reason, even the most luminous starburst galaxies are difficult to observe at optical wavelengths. The absorbed radiation is re-emitted by the dust as long-wavelength infrared radiation, which can easily escape the starforming regions, but cannot cross the Earth's atmosphere. However, for very distant objects this radiation is redshifted to sub-millimeter wavelengths. This makes it accessible from the ground, at a very few places such as Llano de Chajnantor, for telescopes such as APEX. The antenna of APEX has also a diameter of 12 meters, with a reflector surface accuracy of better than 18 micron. It is suitable for observations beyond 1 THz and is designed to give precision performance even with wind speeds up to 9 m/s. The pointing accuracy is specified to be better than 2.0 arcsec.

Conclusion We want to understand better the process behind the formation of super massive black holes and therefore we want more information about young high-redshift black holes. The idea of this small research is determining if it is possible to detect and observe high-redshift black holes with ALMA for

¹The website of APEX: <http://www.mpifr-bonn.mpg.de/div/mm/apex.html>

gaining features of the early quasars in our universe. The conclusion actually consists of two parts:

1. It is possible to *detect* black holes at a high-redshift ($6 \leq z \leq 10$) with the atomic cooling lines [CII]158 and [OI]63 μm using the different bands of ALMA and integrating for at least a few hours.

2. Using the numbers from Schleicher et al. (2008) one can predict ALMA will *detect* about 1 black hole $M_{BH} \geq 10^7 M_{\odot}$ at a redshift of $z = 6$ in a field of view of $(1')^2$.

The overall conclusion is that when ALMA will be full operational it will be able to detect high-redshift black holes using the atomic cooling lines [OI]63 and [CII]158 μm .

Bibliography

- Abel, T., Bryan, G., Norman M. (2000) *The formation and fragmentation of primordial molecular clouds* The Astrophysical Journal (ApJ), 540, 39
- Bromm, V., Loeb, A. (2003) *Formation of the first supermassive black holes* ApJ, 596, 34
- Di Matteo, T., Springel, V., Hernquist, L. (2005) *Energy input from quasars regulates the growth and activity of black holes and their host galaxies* Nature, vol 433
- Fan, X., Narayanan, V., Lupton, R., Strauss, M., Knapp, G., Becker, R., White, R., Pentericci, L., Leggett, S., Haiman, Z., Gunn, J., Ivezić, Ž, Schneider, D., Anderson, S., Brinkmann, J., Bahcall, N., Connolly, A., Csabai, I., Doi, M., Fukugita, M., Geballe, T., Grebel, E., Harbeck, D., Hennessy, G., Lamb, D., Miknaitis, G., Munn, J., Nichol, R., Okamura, S., Pier, J., Prada, F., Richards, G., Szalay, A., York, D. (2001) *A survey of $z > 5.8$ quasars in the sloan digital sky survey* The Astronomical Journal (AJ), 122, 2833
- Häring, N., Rix, H. (2004) *On the black hole mass-bulge mass relation* AJ, 604, L89
- Magorrian, J., Tremaine, S., Richstone, D., Bender, R., Bower, G., Dressler, A., Faber, S., Gebhardt, K., Green, R., Grillmair, C., Kormendy, J., Lauer, T. (1998) *The demography of massive dark objects in galaxy centers* AJ, 115, 2285
- Meijerink, R., Spaans, M. (2005) *Diagnostics of irradiated gas in galaxy nuclei* Astronomy & Astrophysics (A&A), 436, 397
- Mo, H., Mao, S., White, S. (1998) *The formation of galactic discs* Mon. Not. R. Astron. Soc (MNRAS), 295, 319
- Norman, C., Spaans, M. (1997) *Molecules at high redshift: the evolution of the cool phase of protogalactic disks* ApJ, 480, 145
- Press, W., Schechter, P. (1974) *Formation of galaxies and clusters of galaxies by self-similar gravitational condensation* ApJ, 187, 425
- Schleicher, D., Spaans, M., Klessen, R. (2008) *The prospects of finding the first quasars in the universe* ArXiv: 0812.3950

- Sheth, R., Mo, H., Tormen, G. (2001) *Ellipsoidal collapse and an improved model for the number and spatial distribution of dark matter haloes* MNRAS, 323, 1
- Silk, J., Rees, M. (1998) *Quasars and galaxy formation* A&A, 331, L1
- Spaans, M., Meijerink, R. (2008) *On the detection of high-redshift black holes with ALMA through CO and H₂ emission* ApJ, 678, L5
- Spaans, M., Silk, J. (2006) *Pregalactic black hole formation with an atomic hydrogen equation of state* ApJ, 652, 902
- Spinoglio, L., Malkan, M., Smith, H., González-Alfonso, E., Fischer J. (2005) *The far-infrared emission line and continuum spectrum of the Seyfert galaxy NGC 1068* ApJ, 623, 123
- White, S., Frenk, C. (1991) *Galaxy formation through hierarchical clustering* ApJ, 379, 52